

# Theoretical Study on Structural, Electronic, and Optical Properties of Ambipolar Diphenylamino End-capped Oligofluorenylthiophenes and Fluoroarene-thiophene as Light-emitting Materials

Xue-Qin Ran,<sup>†</sup> Ji-Kang Feng,<sup>\*,†,‡</sup> Yan-Ling Liu,<sup>†,‡</sup> Ai-Min Ren,<sup>†</sup> Lu-Yi Zou,<sup>†</sup> and Chia-Chung Sun<sup>†</sup>

State Key Laboratory of Theoretical and Computational Chemistry, Institute of Theoretical Chemistry and the College of Chemistry, Jilin University, Changchun 130023, People's Republic of China

Received: June 24, 2008; Revised Manuscript Received: September 6, 2008

Ambipolar diphenylamino end-capped oligofluorenylthiophenes and fluoroarene-thiophene show great potential for application in organic light-emitting diodes (OLEDs). Here, we provide an in-depth investigation on the optical and electronic properties of OF(2)TP-NPh (**1a**), OF(2)DTP-NPh (**2a**), OF(2)TTP-NPh (**3a**), OF(2)QTP-NPh (**4a**), and 2,5-bis-(2,3,5,6-tetrafluoro-4-trifluoromethyl-phenyl)-2,2':5',2'':5'',2'''-quaterthiophene (**5a**). The geometric and electronic structures of the oligomers in the ground-state are studied with density functional theory (DFT) and ab initio Hartree-Fock, whereas the lowest singlet excited states are optimized by ab initio CIS. The energies of the lowest singlet excited states are calculated by employing time-dependent density functional theory (TDDFT). The results show that the highest occupied molecular orbitals, lowest unoccupied molecular orbitals, energy gaps, ionization potentials, and electron affinities for the oligomers are affected by the thiophene chain length and the different end-caps. The absorption and emission spectra exhibit red shifts to some extent due to the increasing thiophene chain length and the enhancing electron-donating property of the end-caps. Furthermore, the large Stokes shifts ranging from 58 to 80 nm are examined, resulting from a more planar conformation of the excited-state between the two adjacent units in the oligomers. All the calculated data show that the fluoroarene-thiophene has improved electron transport rate and charge transfer balance performance, and all the studied molecules can be used as ambipolar-transporting materials in OLEDs.

## 1. Introduction

Since the advent of a first generation of organic light-emitting diode (OLED) displays in consumer electronics, there have been continuous developments of more efficient and stable multi-functional luminescent materials for the purpose of improving multilayer device fabrication processes and for further enhancing the device performance and stability.<sup>1–3</sup> Among these materials, thiophene-based  $\pi$ -conjugated oligomers have received considerable attention for potential applications in OLEDs that take advantage of their excellent chemical, thermal, and photochemical stabilities as well as ease of structural tuning to adjust the electronic and morphological properties.<sup>4–8</sup> As a result, a number of oligothiophene and polythiophene derivatives have been synthesized and investigated as excellent hole-transporting materials.<sup>9–12</sup> The device performance of OLEDs depends on the charge balance of the injected holes and electrons as well as the exciton confinement in a device. Although the electron-transporting property is relatively rare in thiophene-based  $\pi$ -conjugated materials, it can generally be introduced by incorporation of electron-withdrawing groups such as fluoro, cyano, perfluoroalkyl, perfluoroaryl, and dicyanomethylene into the thiophene system.<sup>13,14</sup>

Recently, for the first time, Wong et al. showed that the oligothiophene moiety can act as an excellent electron-affinitive unit to facilitate electron transport when coupled with diphenylamino end-caps, which can be used to enhance the perfor-

mance of OLEDs.<sup>4,5</sup> In addition to the low first ionization potentials, high thermal stabilities, and good amorphous morphological stabilities, they found that the photoluminescence efficiencies of the D- $\pi$ -A- $\pi$ -D type ambipolar molecules OF(2)TP-NPh, OF(2)DTP-NPh, OF(2)TTP-NPh and OF(2)QTP-NPh have been largely improved. Therefore, it is significant for us to extend our earlier work to a comprehensive theoretical investigation on OF(2)DTP-NPh, OF(2)TTP-NPh, and OF(2)QTP-NPh.<sup>15</sup> To search for new thiophene-based materials with improved electron-transporting performance besides good hole-transporting property, 2,5-bis-(2,3,5,6-tetrafluoro-4-trifluoromethyl-phenyl)-2,2':5',2'':5'',2'''-quaterthiophene (**5a**) was designed, investigated, and compared with OF(2)QTP-NPh, since the incorporation of electron withdrawing groups into the thiophene system may generally favor the electron-accepting and transporting property.<sup>16</sup>

Density functional theory (DFT), single excitation configuration interaction (CIS), and time-dependent density functional theory (TDDFT) calculations have been carried out for the considered molecules. Particular attention was paid to the influence of different end-caps and the chain length of the thiophene core. Highest occupied molecular orbitals (HOMOs), lowest unoccupied molecular orbitals (LUMOs), energy gaps, ionization potentials (IPs), electron affinities (EAs), reorganization energies, and molecular modeling of these molecules indicate that OF(2)TP-NPh (**1a**), OF(2)DTP-NPh (**2a**), OF(2)TTP-NPh (**3a**), OF(2)QTP-NPh (**4a**) and **5a** can exhibit efficient electron transport in addition to hole transport. It has been shown that the designed fluoroarene-thiophene as well as these diphenyl-

\* Corresponding author. E-mail: jikangf@yahoo.com; phone: +86-431-88499856; fax: +86-431-88498026.

<sup>†</sup> Institute of Theoretical Chemistry.

<sup>‡</sup> College of Chemistry.

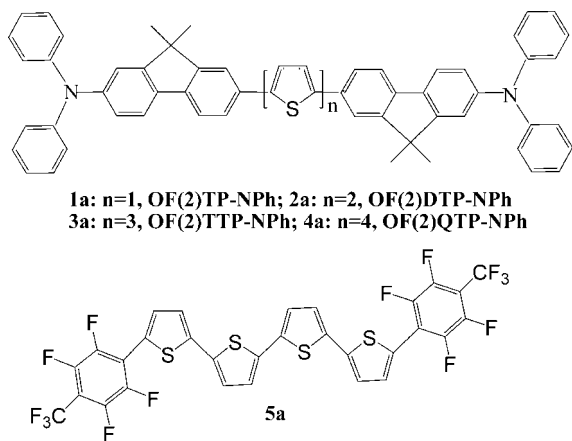


**Figure 1.** Sketch map of the structures of **1a–5a**.

amino end-capped oligofluorenylthiophenes show improved OLED device performance.

## 2. Computational Details

All calculations on the considered molecules have been performed on the SGI origin 2000 server with the Gaussian 03 program package.<sup>17</sup> The ground-state geometries, as well as the cationic and anionic structures of the studied molecules were optimized by DFT//B3LYP/6–31G(d). There is no symmetric constraint on the geometric optimization. CIS/3–21G(d) were employed to calculate the lowest singlet excited-state structures based on the optimized geometries obtained from HF/3–21G(d). The electronic absorption and emission spectra were systematically investigated by the TDDFT method on the basis of each optimized structure. In addition, the various properties of these molecules, such as HOMOs, LUMOs, energy gaps, IPs, EAs, and reorganization energies are obtained from the computed results and are compared with the available experimental data.

## 3. Results and Discussion

**3.1. Ground and Excited Structures.** The sketch map of the structures is depicted in Figure 1, and the optimized geometries obtained by DFT//B3LYP/6–31G(d) of **1a–5a** are plotted in Figure 2. Table 1 and 2 list the important inter-ring bond lengths, dihedral angles, and dipole moments of **1a–5a** calculated by DFT and Hartree–Fock (HF) methods. In contrast to the oligofluorenylthiophenes in the literature,<sup>4,5</sup> **1a–4a** in this contribution substitute butyl with methyl in fluorene rings for the sake of reducing the time of calculation. In addition, the fluoroarene moiety and oligothiophenes in **5a** are abbreviated to  $\pi$  and A, respectively, for simplicity and convenience.

Increasing thiophene chain length in **1a–4a**, the ground-state structures obtained by DFT does not cause appreciable changes. In **5a** and **4a**, the  $\pi$ –A bond lengths and dihedral angles calculated by DFT increase from 1.460 to 1.464 Å and from 6.7° to 24.9°, respectively, to relieve unfavorable steric interactions between diphenylaminofluorenyl moieties and thiophene rings. In the ground state, the DFT calculated results are close to those obtained with the HF approach, except for the  $\pi$ –A bond lengths and dihedral angles in **1a–4a**, which are overestimated by HF.

For the sake of comparison of the ground and excited-state structures, a part of bond lengths and twist angles of the excited structures for **1a–5a** with CIS/3–21G(d) are present in Table 3. The comparison with HF-calculated results indicates that electronic excitation leads to large variations for both inter-

ring bond lengths and dihedral angles, especially for those between  $\pi$  and A. For example, the bond lengths and dihedral angles between  $\pi$  and A in **1a** and **2a** decrease from 1.474 to 1.411 Å, 41.2° to 0.0°, and from 1.474 to 1.430 Å, 41.5° to 0.0°, respectively. This indicates that the singlet excited structures between the two adjacent units in the oligothiophenes should be more planar than their ground structures. Particularly, the inter-ring dihedral angles between A and  $\pi$  in **1a–3a** and **5a** are nearly 0°, implying that the dimethylfluorene and the adjacent thiophene in **1a–3a** and **5a** may be coplanar in the excited state.

Tables 1–3 also list the dipole moment values of **1a–5a**. In the ground state, the HF data are higher than those calculated by DFT. It can be found that the dipole moments of **1a**, **2a**, and **5a** in the excited-state decrease much more than those of **3a** and **4a**. Notably, the dipole moments of **1a** (DFT, 0.63 D; HF, 0.92 D; CIS, 0.50 D) are higher than those of **2a–4a**. This may be attributed to the highly nonplanar conformation of **1a** in comparison with that of **2a–4a**.

**3.2. Frontier Molecular Orbitals.** To characterize the optical and electronic properties, it is useful to examine the HOMOs, LUMOs, and energy gaps. Figure 3 shows the plots of HOMOs and LUMOs for **1a–5a** obtained by DFT//B3LYP/6–31G(d). Table 4 lists the calculated HOMO and LUMO energies and energy gaps, as well as the available experimental results. To more easily and vividly observe the varieties of the HOMOs, LUMOs, and energy gaps, the total density of states (DOS) of **1a–5a** has been compared with each other, as shown in Figure 4.

Theoretically, the energy gap is the orbital energy difference between HOMO and LUMO, termed the HOMO–LUMO gap ( $\Delta E_{\text{H-L}}$ ).<sup>18–20</sup> Experimentally, the most-used band gap is obtained from the absorption spectra, which is the lowest transition (or excitation) energy from the ground-state to the first dipole-allowed excited state, termed the optical band gap ( $E_g$ ). In fact, the optical band gap is not the orbital energy difference between HOMO and LUMO, but the energy difference between the  $S_0$  and  $S_1$  states. Only when the excitation to the  $S_1$  state corresponds almost exclusively to the promotion of the electron from the HOMO to the LUMO can the optical band gap be approximately equal to the HOMO–LUMO gap in quantity. In this contribution, the optical band gaps of **1a–5a** were obtained from the absorption spectra by TDDFT.

As visualized in Figure 3, all the frontier orbitals show  $\pi$  characteristics. Both the HOMOs and LUMOs for **1a–4a** and **5a** consist of linear combinations of individual D,  $\pi$ , and A, and  $\pi$  and A groups, respectively. For **1a–4a**, the HOMO orbitals are spread over the whole conjugated molecules, but the LUMO orbitals are centralized on the dimethylfluorenes and electron affinitive cores. Whereas for **5a** the HOMO orbitals are mainly localized on the thiophenes, the LUMO orbitals are distributed on the whole conjugated molecules. Substantial contribution from the nitrogen atom is also seen in the HOMO orbital plots of **1a–4a**, whereas the fluorine atoms make little direct contribution to either HOMO or LUMO orbitals of **5a**. In general, the HOMO orbitals exhibit bonding character, and the LUMO orbitals hold antibonding character. It is noteworthy that the HOMO orbitals show an antibonding interaction between the two adjacent subunits, D and  $\pi$ , and  $\pi$  and A, and the LUMO orbitals represent the bonding interaction in these regions, consisting of the shortening of the corresponding inter-ring bond lengths in the excited states. Importantly, because the lowest singlet excited-state corresponds almost exclusively to the excitation from the HOMO to the LUMO in all studied

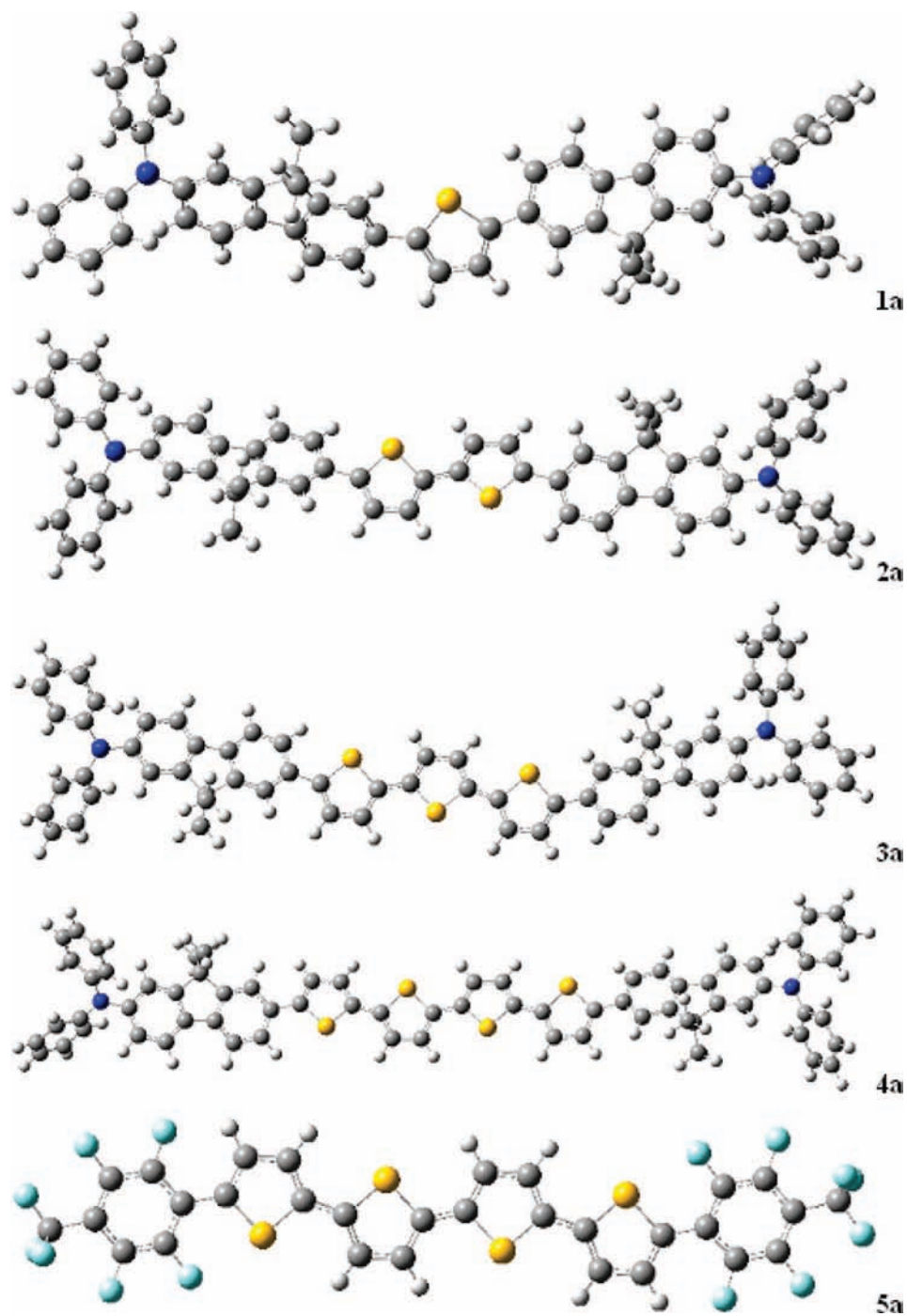


Figure 2. Optimized structures of **1a–5a** by DFT//B3LYP/6–31G(d).

TABLE 1: Selected Important Dihedral Angles and Inter-ring Distances of **1a–5a** in the Ground State with DFT//B3LYP/6–31G(d)<sup>a</sup>

molecule	inter-ring distances (Å)				dihedral angles (°)				dipole moment ( <i>D</i> )
	D– $\pi$	$\pi$ –A	A– $\pi$	$\pi$ –D	D– $\pi$	$\pi$ –A	A– $\pi$	$\pi$ –D	
<b>1a</b>	1.421	1.465	1.465	1.421	42.0	23.8	27.2	41.3	0.63
<b>2a</b>	1.420	1.463	1.463	1.420	40.7	24.2	24.2	40.7	0.14
<b>3a</b>	1.420	1.463	1.463	1.420	41.5	23.6	25.6	40.7	0.46
<b>4a</b>	1.419	1.464	1.463	1.419	40.0	24.9	24.6	40.3	0.18
<b>5a</b>		1.460	1.460			6.7	6.5		0.90

<sup>a</sup> D, diphenylamino;  $\pi$ , dimethylfluorene or phenyl; A, thiophene ring.

molecules (see the Absorption and Emission Spectra section), we can predict the differences of the bond lengths between the ground ( $S_0$ ) and lowest singlet excited state ( $S_1$ ) from MO nodal

patterns. For example, the HOMO orbitals of the studied molecules have nodes between the two adjacent subunits, D and  $\pi$ , and  $\pi$  and A, whereas the LUMO orbitals are bonding

**TABLE 2: Selected Important Dihedral Angles and Interring Distances of 1a–5a in the Ground State with HF/3-21G(d)<sup>a</sup>**

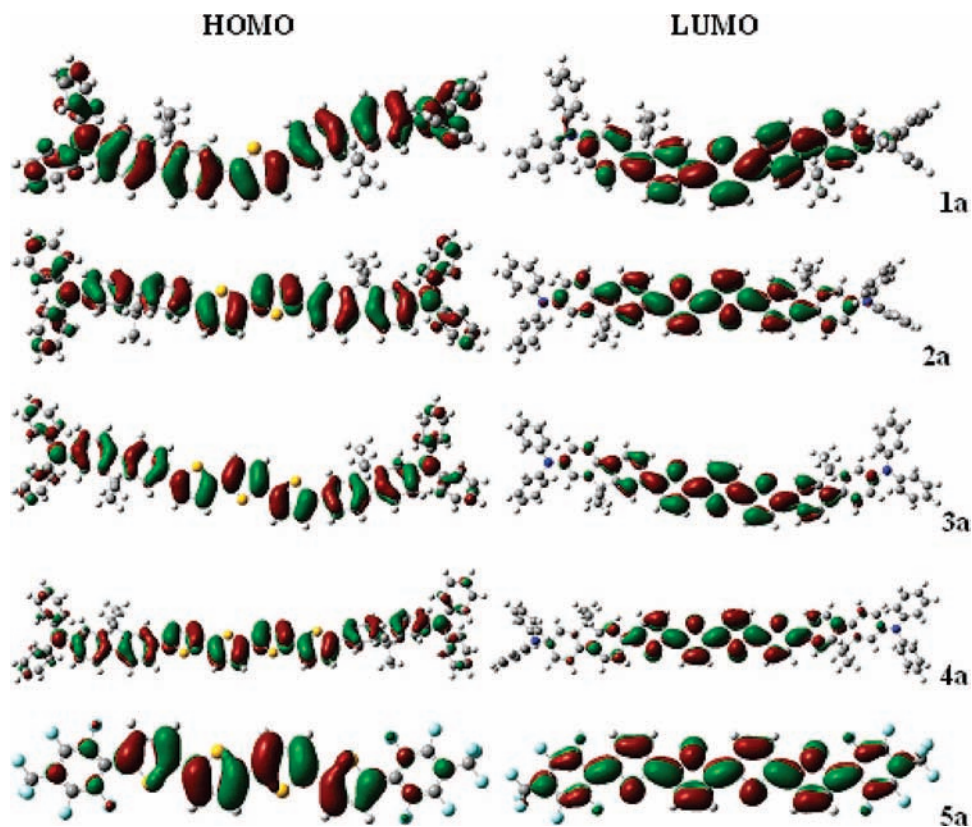
molecule	inter-ring distances (Å)				dihedral angles (deg.)				dipole moment ( <i>D</i> )
	D- $\pi$	$\pi$ -A	A- $\pi$	$\pi$ -D	D- $\pi$	$\pi$ -A	A- $\pi$	$\pi$ -D	
1a	1.421	1.474	1.474	1.421	43.4	41.2	41.9	44.3	0.92
2a	1.421	1.474	1.474	1.421	43.0	41.5	42.3	42.8	0.32
3a	1.421	1.474	1.474	1.421	42.7	41.6	41.7	42.7	0.54
4a	1.421	1.474	1.474	1.421	42.5	41.6	42.4	42.6	0.18
5a		1.463	1.463			0.2	0.2		2.69

<sup>a</sup> D, diphenylamino;  $\pi$ , dimethylfluorene or phenyl; A, thiophene ring.

**TABLE 3: Selected Important Dihedral Angles and Interring Distances of 1a–5a in the Excited State with CIS/3-21G(d)<sup>a</sup>**

molecule	inter-ring distances (Å)				dihedral angles (deg.)				dipole moment ( <i>D</i> )
	D- $\pi$	$\pi$ -A	A- $\pi$	$\pi$ -D	D- $\pi$	$\pi$ -A	A- $\pi$	$\pi$ -D	
1a	1.415	1.411	1.411	1.415	38.8	0.0	0.0	38.9	0.50
2a	1.417	1.430	1.430	1.417	40.0	0.0	0.0	40.0	0.00
3a	1.419	1.446	1.444	1.418	40.8	8.5	0.1	40.7	0.49
4a	1.419	1.458	1.458	1.419	41.4	24.0	23.8	41.4	0.42
5a		1.447	1.447			0.0	0.0		0.00

<sup>a</sup> D, diphenylamino;  $\pi$ , dimethylfluorene; A, thiophene ring.

**Figure 3.** Plots of HOMO and LUMO of 1a–5a by DFT//B3LYP/6–31G(d).**TABLE 4: Negative of the HOMO ( $-\epsilon_{\text{HOMO}}$ ) and LUMO Energies ( $-\epsilon_{\text{LUMO}}$ ), HOMO–LUMO Gaps Calculated by DFT, and the Lowest Excited Energies Calculated by TD-DFT (in eV) for 1a–5a**

molecule	$-\epsilon_{\text{HOMO}}$	$-\epsilon_{\text{HOMO}}$ (exp)	$-\epsilon_{\text{LUMO}}$	$-\epsilon_{\text{LUMO}}$ (exp)	$\Delta E_{\text{H-L}}$	$E_{\text{g}}$	$E_{\text{g}}$ (exp)
1a	4.68	5.14	1.50	2.39	3.18	2.80	2.75
2a	4.66	5.12	1.73	2.51	2.93	2.58	2.61
3a	4.65	5.11	1.89	2.60	2.76	2.43	2.51
4a	4.64	5.11	1.99	2.73	2.65	2.32	2.39
5a	5.40		2.71		2.69	2.43	

in these regions. As a result, we can expect the contraction of these inter-ring bond lengths. The data in Table 3 confirm that these inter-ring bond lengths become considerably shorter in the excited-state as discussed earlier.

As shown in Table 4 and Figure 4, the calculated HOMO and LUMO energies and energy gaps have the same variation trends with the available experimental results, with the largest deviation of 0.89 eV in value. From 1a to 4a, the HOMO

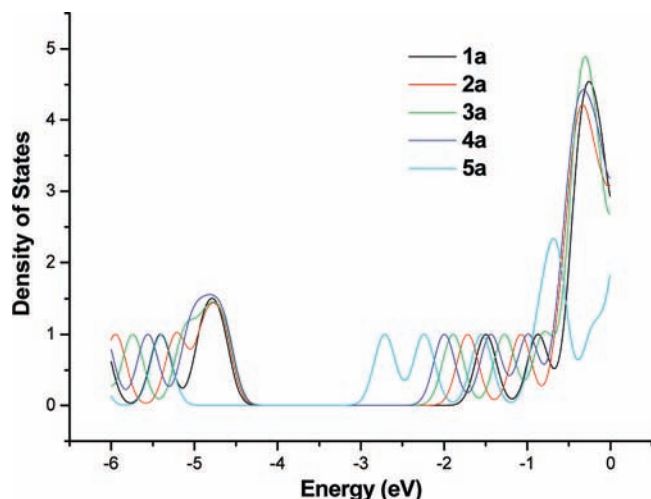


Figure 4. Total of density of states of **1a–5a**.

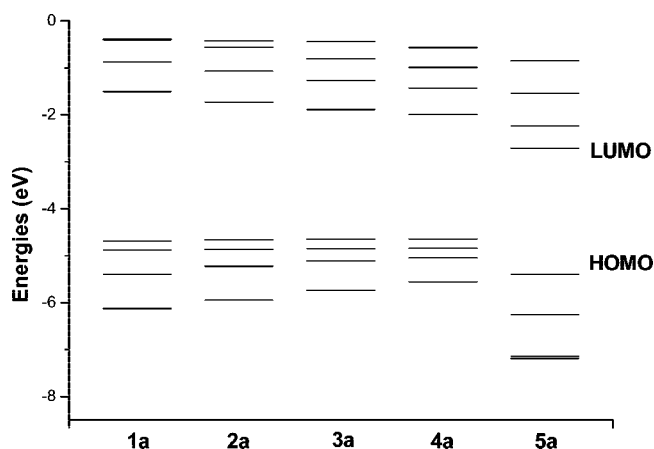


Figure 5. Sets of one-electron energy levels of **1a–5a** by DFT//B3LYP/6–31G(d).

energies slightly increase, and the LUMO energies greatly decrease. This indicates that hole-creating and electron-accepting abilities have been largely improved when the conjugated length of the thiophene core increases. Also, such a high HOMO energy level (−4.68 to −4.64 eV) and a low LUMO energy level (−1.99 to −1.50 eV) largely reduce the energy barrier for the hole creation and electron acceptance. That is to say, the ability of charge injection becomes enhanced from **1a** to **4a**. When compared with that of **5a**, we find that the LUMO energy is higher in **4a**, implying that the substitution of the strong electron donating diphenylaminofluorenyl moiety with an electron accepting fluoroarene greatly improves the electron acceptance.

To more easily observe the change of the HOMO and LUMO energies, sets of one-electron energy levels of **1a–5a** (from HOMO<sub>−3</sub> to LUMO<sub>+3</sub>) are plotted in Figure 5. It can be seen in Figure 5 that the energy difference between HOMO and HOMO<sub>−1</sub>, LUMO and LUMO<sub>+1</sub> orbital for **1a–4a** is small. For example, the HOMO (−4.64 eV) lies 0.2 eV higher in energy than the HOMO<sub>−1</sub> orbital (−4.84 eV) in **4a**, whereas the LUMO<sub>+1</sub> orbital energy (−1.43 eV) is 0.56 eV larger than LUMO (−1.99 eV). For **5a**, the energy difference between LUMO (−2.71 eV) and LUMO<sub>+1</sub> orbital (−2.23 eV) is 0.48 eV, but the HOMO (−5.40 eV) and HOMO<sub>−1</sub> orbital (−6.26 eV) have a larger split. It implies that it is possible to promote an electron from the HOMO<sub>−1</sub> to LUMO or LUMO<sub>+1</sub>, or from the HOMO to LUMO<sub>+1</sub> in **1a–4a**, and from the HOMO to LUMO<sub>+1</sub> in **5a**, except for the HOMO → LUMO transition (see Absorption and Emission Spectra section).

TABLE 5: Ionization Potentials, Electronic Affinities, Extraction Potentials, and Reorganization Energies for Each Molecule (in eV) Calculated by DFT//B3LYP/6-31G(d)

molecule	IP(v)	IP(a)	HEP	EA(v)	EA(a)	EEP	$\lambda_{\text{hole}}$	$\lambda_{\text{electron}}$
<b>1a</b>	5.50	5.38	5.27	0.53	0.77	0.96	0.23	0.43
<b>2a</b>	5.43	5.33	5.21	0.78	0.99	1.18	0.22	0.40
<b>3a</b>	5.38	5.28	5.18	0.96	1.16	1.32	0.20	0.36
<b>4a</b>	5.34	5.25	5.16	1.10	1.29	1.45	0.18	0.35
<b>5a</b>	6.47	6.33	6.20	1.72	1.88	2.04	0.27	0.32

As observed in Table 4, the energy gap becomes narrower from **1a** to **4a**, which can be expected from the increasing HOMO energies and decreasing LUMO energies from **1a** to **4a**. From this we can predict the red-shifted absorption and emission wavelengths when increase the conjugated length of the thiophene core. However, the energy gap level of **5a** is larger than that of **4a**, resulting from the influence of the electron-withdrawing moiety.

By the above discussion we find that the HOMOs, LUMOs, and energy gaps (both  $\Delta E_{\text{H-L}}$  and  $E_g$ ) are affected by the conjugated length of the thiophene core and the different end-caps. The longer the conjugated length, the higher the HOMO energies, the lower the LUMO energies, and the narrower the energy gaps. However, the stronger electron-withdrawing strength of the end-caps leads to the lower HOMO and LUMO energies. Then we can predict the absorption and emission spectra from the orbital properties.

**3.3. Ionization Potentials and Electronic Affinities.** As mentioned in the Introduction, the device performance of OLEDs depends on the charge injection, transfer, and balance as well as the exciton confinement in a device. So it is important to investigate the IP, EA, and reorganization energy ( $\lambda$ ), which can be used to evaluate the energy barrier for the injection of holes and electrons, and the charge transfer (or transport) rate and balance. The DFT calculated IP, EA, and reorganization energy ( $\lambda$ ), as well as hole extraction potential and electron extraction potential for **1a–5a** are listed in Table 5. The IP and EA can be either for vertical excitations (v; at the geometry of the neutral molecule) or adiabatic excitations (a; optimized structure for both the neutral and charged molecule). In addition, HEP is the energy difference from M (neutral molecule) to M<sup>+</sup> (cationic), using M<sup>+</sup> geometric structure in the calculation, and EEP is the energy difference from M to M<sup>−</sup> (anionic), using M<sup>−</sup> geometric structure in the calculation.

As observed from Tables 5 and 4, the variety of trends of the IP and EA for **1a–5a** is the same with those of the negative of HOMO and LUMO energies. For **1a–4a**, it can be seen that the EA values increase sharply (0.77~1.29 eV), whereas the IP values decrease slightly (5.50~5.34 eV) with increasing thiophene chain length. This indicates that the abilities to accept an electron and to create a hole have been improved from **1a** to **4a**, especially the electron-acceptance ability. In addition, the EA and IP values of **5a** (1.88 and 6.47 eV, respectively) are

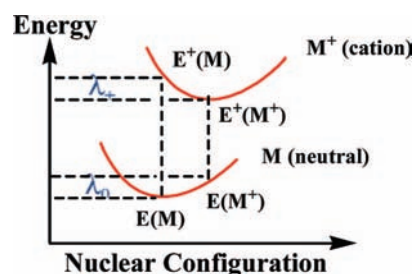


Figure 6. Internal reorganization energy for hole transfer.

**TABLE 6: Electronic Transition Data Obtained by TD-DFT ( $\lambda_{\text{abs,max}}$ ) for **1a–5a** at the B3LYP/6-31G(d) Optimized Geometry**

molecule	electronic transitions	$\lambda_{\text{abs,max}}$ (nm)	$\text{exp}^a \lambda_{\text{abs}}$	$f$	$\text{exp}^a f$	transition moment	main configurations	
<b>1a</b>	$S_0 \rightarrow S_1$	440.56	390	1.9744	7.29	5.35	HOMO <sub>-1</sub> $\rightarrow$ LUMO <sub>+1</sub>	0.110.67
	$S_0 \rightarrow S_2$	399.56		0.0336			HOMO $\rightarrow$ LUMO	
	$S_0 \rightarrow S_3$	353.73		0.0560			HOMO <sub>-1</sub> $\rightarrow$ LUMO	0.69
<b>2a</b>	$S_0 \rightarrow S_1$	476.70	424	2.4555	7.00	6.21	HOMO <sub>-1</sub> $\rightarrow$ LUMO <sub>+1</sub>	0.110.67
	$S_0 \rightarrow S_2$	426.90		0.0047			HOMO <sub>-1</sub> $\rightarrow$ LUMO	0.69
	$S_0 \rightarrow S_3$	382.26		0.3400			HOMO <sub>-2</sub> $\rightarrow$ LUMO	0.67
<b>3a</b>	$S_0 \rightarrow S_1$	510.86	441	2.6682	6.76	6.70	HOMO <sub>-1</sub> $\rightarrow$ LUMO <sub>+1</sub>	0.11 0.66
	$S_0 \rightarrow S_2$	453.44		0.0183			HOMO <sub>-1</sub> $\rightarrow$ LUMO	0.69
	$S_0 \rightarrow S_3$	414.06		0.2777			HOMO <sub>-2</sub> $\rightarrow$ LUMO	0.67
<b>4a</b>	$S_0 \rightarrow S_1$	534.09	451	3.0398	6.74	7.31	HOMO <sub>-1</sub> $\rightarrow$ LUMO <sub>+1</sub>	0.11 0.66
	$S_0 \rightarrow S_2$	471.66		0.0094			HOMO <sub>-1</sub> $\rightarrow$ LUMO	0.69
	$S_0 \rightarrow S_3$	435.86		0.2320			HOMO <sub>-2</sub> $\rightarrow$ LUMO	0.68
<b>5a</b>	$S_0 \rightarrow S_1$	511.06		2.1303		5.98	HOMO $\rightarrow$ LUMO	0.65
	$S_0 \rightarrow S_2$	429.18		0.0012			HOMO <sub>-1</sub> $\rightarrow$ LUMO	0.270.64
	$S_0 \rightarrow S_3$	367.07		0.0049			HOMO <sub>-1</sub> $\rightarrow$ LUMO	0.610.20
							HOMO $\rightarrow$ LUMO <sub>+1</sub>	

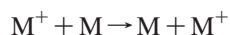
<sup>a</sup> Measured in CHCl<sub>3</sub> (ref. 17).

**TABLE 7: Emission Data Obtained by TD-DFT for **1a–5a** at the CIS/3-21G(d) Optimized Geometry**

molecule	electronic transitions	$\lambda^{\text{em}}$ (nm)	exp	$f$	$E$ (eV)	main configurations	$\tau$ (ns)	$\tau$ (ns,exp)	
<b>1a</b>	$S_0 \rightarrow S_1$	517.80	487	2.3711	2.39	HOMO $\rightarrow$ LUMO	0.65	1.71	1.14
<b>2a</b>	$S_0 \rightarrow S_1$	556.30	525	2.7384	2.23	HOMO $\rightarrow$ LUMO	0.64	1.70	0.71
<b>3a</b>	$S_0 \rightarrow S_1$	586.23	540	2.9001	2.11	HOMO $\rightarrow$ LUMO	0.63	1.79	1.19
<b>4a</b>	$S_0 \rightarrow S_1$	592.06	560	3.1560	2.09	HOMO $\rightarrow$ LUMO	0.63	1.68	1.21
<b>5a</b>	$S_0 \rightarrow S_1$	570.68		2.2974	2.17	HOMO $\rightarrow$ LUMO	0.62	2.14	

much larger than those of **4a**, indicating that only the electron acceptance ability of **5a** has been greatly enhanced. These investigations are in accord with the analysis from the HOMO and LUMO energies and provide an in-depth interpretation of the electronic properties of these oligothiophenes.

In general, organic  $\pi$ -conjugated materials are assumed to transport charge at room temperature via a thermally activated hopping-type mechanism.<sup>21–24</sup> As the vast majority of these organic conductive materials are p-type, the hole-transfer process between adjacent spatially separated segments can be summarized as follows:



where M represents the neutral species undergoing charge transfer, and the M<sup>+</sup> species contains the hole. If the temperature is sufficiently high to treat vibrational modes classically, then the standard Marcus/Hush model yields the following expression for the hole (or electron) charge transfer rate,<sup>25–28</sup> assuming that hole traps are degenerate:

$$k_{\text{hole}} = \left( \frac{\pi}{\lambda k_B T} \right)^{1/2} \frac{V^2}{\hbar} \exp\left( -\frac{\lambda}{4k_B T} \right) \quad (1)$$

where  $T$  is the temperature,  $k_B$  is the Boltzmann constant,  $\lambda$  is the reorganization energy due to geometric relaxation accompanying charge transfer, and  $V$  is the electronic coupling matrix element between the two species, dictated largely by orbital overlap. Obviously,  $\lambda$  and  $V$  are the two most pivotal parameters and have a dominant impact on the charge-transfer rate, especially the former. Then we mainly investigate the reorganization energy for **1a–5a**. Here, the reorganization energy is just the internal reorganization energy of the isolated active organic  $\pi$ -conjugated systems due to ignoring any

environmental relaxation and changes. Hence, the reorganization energy for hole transfer in eq 1 can be defined as follows;<sup>24</sup>

$$\lambda_{\text{hole}} = \lambda_+ + \lambda_0 = [E^+(M) - E^+(M^+)] + [E(M^+) - E(M)]$$

$$= [E^+(M) - E(M)] - [E^+(M^+) - E(M^+)] = \text{IP}(v) - \text{HEP} \quad (2)$$

As illustrated in Figure 6,  $E(M)$  and  $E^+(M^+)$  represent the energies of the neutral and cation species in their lowest energy geometries, respectively, whereas  $E(M^+)$  and  $E^+(M)$  represent the energies of the neutral and cation species with the geometries of the cation and neutral species, respectively. This description holds as long as the potential energy surfaces are harmonic and the  $\lambda_0$  and  $\lambda_+$  terms are close in energy. It is known that many factors, including heteroatom identity, heterocycle substituents, and conjugation length, are important in dictating the reorganization energy.

For emitting-layer materials, it needs to achieve the balance between hole injection and electron acceptance. Furthermore, the lower the  $\lambda$  values, the bigger the charge-transport rate. The data in Table 5 show that the  $\lambda_{\text{hole}}$ s for **1a–4a** are all smaller than their respective  $\lambda_{\text{electron}}$ s, suggesting that the hole transfer rate is higher than the electron transfer rate. To improve the electron-transportation, **5a** was designed. It can be seen in Table 5 that the  $\lambda_{\text{electron}}$  and  $\lambda_{\text{hole}}$  of **5a** are smaller and larger, respectively, than that of **4a**, implying that **5a** has better electron transfer rate than **4a**. Although the hole transfer rate of **5a** is smaller than that of **4a**, the small difference between  $\lambda_{\text{electron}}$  (0.32) and  $\lambda_{\text{hole}}$  (0.27) in **5a** shows that **5a** has improved charge transfer (or transport) balance performance. Therefore, the fluoroarene-thiophene oligomer is a better emitter with high quantum efficiency. As observed in Table 5, the reorganization energy decreases from **1a** to **4a** with increasing thiophene chain

length, indicating that the charge transfer rate increases from **1a** to **4a**. The difference between the  $\lambda_{\text{hole}}$  and  $\lambda_{\text{electron}}$  for **1a–5a** is 0.20, 0.18, 0.16, 0.17, and 0.05 eV, respectively, which is small enough that these oligomers can act as nice ambipolar materials with relatively high light emitting efficiencies. Moreover, this indicates that the balance between hole-transfer and electron-transfer as well as the production of the exciton are enhanced from **1a** to **2a**, to **3a**, to **4a**, and then to **5a**. Thus, the effective luminescence is enhanced. As a result, the order of the light emitting efficiencies of these oligomers is **5a** > **4a** > **3a** > **2a** > **1a**.

**3.4. Absorption and Emission Spectra.** TDDFT//B3LYP/6–31G(d) has been employed to investigate the absorption and emission spectra of **1a–5a**. The transition energies, oscillator strengths, and main configurations for the most relevant singlet excited states in each molecule are listed in Tables 6 and 7, respectively. For the absorption spectra, the calculated data for **1a–4a** have the same variation trend with the experimental results. All the electronic transitions are of  $\pi \rightarrow \pi^*$  type, and the strongest absorption peaks with largest oscillator strengths for **1a–5a** arise exclusively from  $S_0 \rightarrow S_1$ , which corresponds to the promotion of an electron from the HOMO to the LUMO. As shown in Table 6, the absorption spectra exhibit red shifts to some extent from **1a** to **4a** due to the increasing thiophene chain length, which confirms the prediction from the energy gap discussed above. The absorption wavelength of **5a** (511.06 nm) is smaller than that of **4a**, also consistent with the variety of the energy gap. It is known that the transition moment is proportional to the oscillator strength<sup>29</sup> for an electronic transition and reflects the transition probability from the ground-state to the excited state. The transition moments and the largest oscillator strength in **1a–5a** (**1a**, 5.35, 1.9744; **2a**, 6.21, 2.4555; **3a**, 6.70, 2.6682; **4a**, 7.31, 3.0398; **5a**, 5.98, 2.1303) indicates that the transition probabilities becomes higher in the order **1a**  $\rightarrow$  **5a**  $\rightarrow$  **2a**  $\rightarrow$  **3a**  $\rightarrow$  **4a**.

For the emission spectra, the emission peaks with the largest oscillator strength for **1a–5a** are all assigned to  $\pi \rightarrow \pi^*$  character, arising from the  $S_1$ , HOMO  $\rightarrow$  LUMO transition. As in the case of the absorption spectra, the emission wavelengths for **1a–5a** exhibit red-shifts in the following order: **1a**  $\rightarrow$  **2a**  $\rightarrow$  **3a**  $\rightarrow$  **5a**  $\rightarrow$  **4a**. The large Stokes shifts ranging from 58 to 80 nm may be explained by a more planar conformation of the excited-state of the considered oligomers. Also, the high oscillator strengths of the  $S_1 \rightarrow S_0$  transitions for **1a–5a** imply that they have large fluorescent intensity and that they are useful as fluorescent OLED materials.

Table 7 also lists the emission lifetimes ( $\tau$ ) calculated for spontaneous emission using the Einstein transition probabilities according to the following formula (in au),<sup>30,31</sup>

$$\tau = \frac{c^3}{2(E_{\text{Flu}})^2 f}$$

where  $c$  is the velocity of light,  $E_{\text{Flu}}$  is the transition energy, and  $f$  is the oscillator strength. The data of  $E_{\text{Flu}}$  and  $f$  are also shown in Table 7. The calculated lifetimes for the oligofluorenylthiophenes (1.71, 1.70, 1.79, and 1.68 ns) have the same order of magnitude with the experimental results (1.14, 0.71, 1.19, and 1.21 ns) with the largest deviation of 0.99 ns in value. By the substitution of diphenylaminofluorenyl moieties with fluoroarene, the lifetime of **5a** is larger than that of **4a**. Here, the discussion further supports the influence of the conjugated thiophene chain length and the electron-withdrawing strength

of the end-caps on the optical and electronic properties of the thiophene-based oligomers.

#### 4. Conclusions

A comprehensive investigation on the oligofluorenylthiophenes has been performed due to their great potential for application in OLEDs. The fluoroarene-thiophene oligomer was designed and studied as a comparison. Necessarily, the structures in the ground-state have been compared with those of the excited-state to trace the structural varies. The calculated results show that the conjugated thiophene chain length and the electron-withdrawing (or donating) character of the end-caps strongly influence the optical and electronic properties. With the thiophene chain length increasing, the HOMOs and EAs increase, whereas the LUMOs, energy gaps, IPs, and reorganization energies decrease, in accord with the improved charge injection and transport balance from **1a** to **4a**. The HOMOs and LUMOs decrease, but energy gaps, IPs and EAs increase with the electron-donating end-caps replaced by electron-withdrawing moieties, consistent with the improved electron-accepting ability found in the fluoroarene-thiophene oligomer. The narrow differences between the  $\lambda_{\text{hole}}$ s and  $\lambda_{\text{electron}}$ s were found in the studied molecules, especially the fluoroarene-thiophene oligomer, which has small  $\lambda_{\text{electron}}$  and improved electron-transporting rate. Moreover, the absorption and emission spectra exhibit red shifts to some extent due to the increasing thiophene chain length. The Stokes shifts ranging from 58 to 80 nm and the large fluorescent lifetimes for all molecules were also reported. Consequently, it can be concluded that the oligomers, particularly the designed molecule, can be used in OLEDs as excellent ambipolar materials. Finally, we are convinced that our work should contribute to orientate the synthesis efforts and help understand the structure–properties relation of these conjugated materials.

**Acknowledgment.** This work is supported by the Major State Basic Research Development Program (2002CB 613406), the National Natural Science Foundation of China (Project No. 20673045), the Science Foundation of Jilin University, and the State Key Laboratory for Supermolecular Structure and Material of Jilin University.

#### References and Notes

- Friend, R. H.; Gymer, R. W.; Holmes, A. B.; Burroughes, J. H.; Marks, R. N.; Taliani, C.; Bradley, D. D. C.; Dos Santos, D. A.; Brédas, J. L.; Lögdlund, M.; Salaneck, W. R. *Nature* **1999**, *397*, 121–128.
- Segura, J. L.; Martin, N. *J. Mater. Chem.* **2000**, *10*, 2403–2453.
- Mitschke, U.; Bäuerle, P. *J. Mater. Chem.* **2000**, *10*, 1471–1507.
- Li, Z. H.; Wong, M. S.; Tao, Y.; Fukutani, H. *Org. Lett.* **2007**, *9*, 3659–3662.
- Li, Z. H.; Wong, M. S.; Fukutani, H.; Tao, Y. *Chem. Mater.* **2005**, *17*, 5032–5040.
- Yoon, M.-H.; Facchetti, A.; Stern, C. E.; Marks, T. J. *J. Am. Chem. Soc.* **2006**, *128*, 5792–5801.
- Koh, S. E.; Delley, B.; Medvedeva, J. E.; Facchetti, A.; Freeman, A. J.; Marks, T. J.; Ratner, M. A. *J. Phys. Chem. B* **2006**, *110*, 24361–24370.
- Koh, S. E.; Risko, C.; da Silva Filho, D. A.; Kwon, O.; Facchetti, A.; Brédas, J.-L.; Marks, T. J.; Ratner, M. A. *Adv. Funct. Mater.* **2008**, *18*, 332–340.
- Vigalok, A.; Swager, T. M. *Adv. Mater.* **2002**, *14*, 368–371.
- Edder, C.; Fréchet, J. M. *Org. Lett.* **2003**, *5*, 1879–1882.
- Horowitz, G. *Adv. Mater.* **1998**, *10*, 365–377.
- Li, W.; Katz, H. E.; Lovinger, A. J.; Laquindanum, J. G. *Chem. Mater.* **1999**, *11*, 458–465.
- Facchetti, A.; Mushrush; Katz, H. E.; Marks, T. J. *Adv. Mater.* **2003**, *15*, 33–38.

- (14) Pappenfus, T. M.; Chesterfield, R. J.; Frisbie, C. D.; Mann, K. R.; Casado, J.; Raff, J. D.; Miller, L. L. *J. Am. Chem. Soc.* **2002**, *124*, 4184–4185.
- (15) Liu, Y.-L.; Feng, J.-K.; Ren, A.-M. *J. Phys. Org. Chem.* **2007**, *20*, 600–609.
- (16) Zhou, G.; Ho, C.-L.; Wong, W.-Y.; Wang, Q.; Ma, D.; Wang, L.; Lin, Z.; Marder, T. B.; Beeby, A. *Adv. Funct. Mater.* **2008**, *18*, 499–511.
- (17) Frisch, M. J.; Trucks, G. W.; Schlegel, H. B.; Scuseria, G. E.; Robb, M. A.; Cheeseman, J. R.; Montgomery, J. A., Jr.; Vreven, T.; Kudin, K. N.; Burant, J. C.; Millam, J. M.; Iyengar, S. S.; Tomasi, J.; Barone, V.; Mennucci, B.; Cossi, M.; Scalmani, G.; Rega, N.; Petersson, G. A.; Nakatsuji, H.; Hada, M.; Ehara, M.; Toyota, K.; Fukuda, R.; Hasegawa, J.; Ishida, M.; Nakajima, T.; Honda, Y.; Kitao, O.; Nakai, H.; Klene, M.; Li, X.; Knox, J. E.; Hratchian, H. P.; Cross, J. B.; Adamo, C.; Jaramillo, J.; Gomperts, R.; Stratmann, R. E.; Yazyev, O.; Austin, A. J.; Cammi, R.; Pomelli, C.; Ochterski, J. W.; Ayala, P. Y.; Morokuma, K.; Voth, G. A.; Salvador, P.; Dannenberg, J. J.; Zakrzewski, V. G.; Dapprich, S.; Daniels, A. D.; Strain, M. C.; Farkas, O.; Malick, D. K.; Rabuck, A. D.; Raghavachari, K.; Foresman, J. B.; Ortiz, J. V.; Cui, Q.; Baboul, I.; Martin, R. L.; Fox, D. J.; Keith, T.; Al-Laham, M. A.; Peng, C. Y.; Nanayakkara, A.; Challacombe, M.; Gill, P. M. W.; Johnson, B.; Chen, W.; Wong, M. W.; Gonzalez, C.; Pople, J. A. *Gaussian 03*, Revision B.04; Gaussian, Inc.: Pittsburgh, PA, 2003.
- (18) Hay, P. J. *J. Phys. Chem. A* **2002**, *106*, 1634–1641.
- (19) Curioni, A.; reoni, W.; Treusch, R.; Himpfel, F. J.; Haskal, E.; Seidler, P.; Heske, C.; Kakar, S.; van Buren, T.; Terminello, L. *J. Appl. Phys. Lett.* **1998**, *72*, 1575–1577.
- (20) Hong, S. Y.; Kim, D. Y.; Kim, C. Y.; Hoffmann, R. *Macromolecules* **2001**, *34*, 6474–6481.
- (21) Epstein, A. J.; Lee, W. P.; Prigodin, V. N. *Synth. Met.* **2001**, *117*, 9.
- (22) Reedijk, J. A.; Martens, H. C. F.; van Bohemen, S. M. C.; Hilt, O.; Brom, H. B.; Michels, M. A. *J. Synth. Met.* **1999**, *101*, 475–476.
- (23) Mott, N. F.; Davis, E. A. *Electronic Processes in Non-Crystalline Materials*, 2nd ed.; Oxford University Press: Oxford, 1979.
- (24) Hutchison, G. R.; Ratner, M. A.; Marks, T. J. *J. Am. Chem. Soc.* **2005**, *127*, 2339–2350.
- (25) Marcus, R. A. *Rev. Mod. Phys.* **1993**, *65*, 599–610.
- (26) Marcus, R. A.; Eyring, H. *Annu. Rev. Phys. Chem.* **1964**, *15*, 155–196.
- (27) Hush, N. S. *J. Chem. Phys.* **1958**, *28*, 962–972.
- (28) Marcus, R. A. *J. Chem. Phys.* **1956**, *24*, 966–978.
- (29) Peyerimhoff, S. D. In *The Encyclopedia of Computational Chemistry*; Schleyer, P. von R., Allinger, N. L., Clark, T., Gasteiger, J., Kollman, P. A., Schaefer, H. F., III, Schreiners, P. R., Eds.; Wiley: Chichester, U. K., 1998; pp 2646–2664.
- (30) Litani-Barzilai, I.; Bulatov, V.; Schechter, I. *Anal. Chim. Acta* **2004**, *501*, 151–156.
- (31) Lukeš, V.; Aquino, A.; Lischka, H. *J. Phys. Chem. A* **2005**, *109*, 10232–10238.

JP805553E